A new Finite Element Technology for the Numerical Simulation of High Speed Forming Processes

S. Reese[1], C. Leppin[2]

[1]Institute of Mechanics, Ruhr University Bochum, Germany;
[2]Alcan Technology & Management Ltd, Neuhausen, Switzerland

Abstract

In this contribution we propose a new solid-shell element formulation based on the concept of reduced integration with hourglass stabilization. Due to the absence of shear locking thin structures can be computed with only one element layer over the thickness. This enhances the computational efficiency in two ways. First of all the number of elements is reduced. Secondly, working with an explicit scheme, a larger critical time step is obtained. The damping and the mass matrix are not affected by the element technological treatment. The formulation is validated at first by typical element examples as well as two forming simulations.

1 Introduction

The numerical simulation of high speed forming processes demands high standards of finite element technology because the workpieces undergo extreme bending whereas the material is plastically incompressible. Especially in these situations standard low order finite element formulations exhibit the undesirable effect of locking. Consequences of this problem are too high stress values and an underestimation of the deformation. Obviously, if the finite element analysis is expected to support the production process by means of quantitatively reliable results the locking must be eliminated. One possibility is to work with higher order elements. However, such formulations require complicated meshing procedures and the coupling with contact algorithms is difficult. Another idea is to enrich the standard displacement-based low order formulation with additional modes in such a way that non-physical constraints (which are the basis for the locking) no longer appear. This so-called method of incompatible modes (or enhanced strain method in more modern terms) is based on a mixed variational principle, i.e. the so-called incompatible strain and the stress act as additional independent variables [1-4]. Formulations of this kind have the disadvantage that internal element variables have to be additionally determined. So their use leads to higher computational cost. In addition, numerical instabilities are frequently encountered in compressive deformation states.

Recently, several authors [5-12] have worked on the problem to transfer the enhanced strain method into finite element formulations based on reduced integration with hourglass

stabilization. It is well-known that such elements, see e. g. the Flanagan-Belytschko approach implemented into ABAQUS, show the important advantages of low numerical cost (in particular in explicit simulations) and robust deformation behaviour. Earlier approaches of this kind, as for instance the just mentioned one, have, however, suffered from the problematic facts that (I) the solution depends on a user-defined parameter and (II) the performance in bending is not satisfactory.

These difficulties are now overcome in the here proposed solid-shell approach (see also [12]) where additionally the "dynamic contributions", i. e. mass and damping terms, have been incorporated. In the suggested new formation the computation of these matrices can be performed in the same way as in the standard displacement approach. The dynamic simulation therefore poses hardly any additional coding effort. The keypoint of the new formulation is the Taylor expansion of the relevant stress quantity (usually the first Piola-Kirchhoff stress tensor) with respect to the normal through the centre of the element. In this way the original nine internal element variables can be reduced to three. Further the integration over the element volume reduces to an integration in thickness direction. Therefore only two Gauss points are needed in total which makes the element very efficient from the computational point of view. Certainly for certain applications it is recommended to work with several Gauss points over the thickness. Important is also the fact that the element, although it is able to exhibit the typical shell-like behaviour, has still eight nodes which are associated solely to *displacement* degrees-of-freedom. For this reason it is very suitable to be used in contact problems and can be easily coupled to classical solid elements. In contrast to many other shell formulations, no assumptions about the kinematics or the stress state are needed. So we are able to model a full three-dimensional stress state. Consequently, continuum mechanical material laws can be implemented without modification. It should also be emphasized that in explicit simulations the computational effort is proportional to the number of Gauss points. If we need only two Gauss points instead of eight in one element, the numerical cost is reduced by 75 $\%$.

In the present contribution we investigate the high speed forming of an axisymmetric workpiece by means of an implicit simulation where also the contact with the blankholder is taken into account. A similar computation has been carried out in [13], however with a different element technology. Questions such as convergence behaviour, robustness, computational efficiency, time stepping are discussed. The results show that the new element formulation has the potential to develop into an excellent tool for practical high speed forming simulations.

2 Variational functional

The present stabilization technique is strongly related to the enhanced strain method (EAS method) of Simo & Armero [1] whose formulation is based on the Hu-Washizu variational functional. To extend their approach to dynamics, we state the three equations

$$\begin{array}{lllcll} \text{(I)} & \text{balance of linear momentum} & : & \operatorname{Div}\mathbf{P} + \rho_0\left(\mathbf{b}_v - \ddot{\mathbf{u}}\right) & = & \mathbf{0} \\ \text{(II)} & \text{constitutive equation} & : & \mathbf{P} - \dfrac{\partial W}{\partial \mathbf{H}} - \mathcal{A}_d : \dot{\mathbf{H}} & = & \mathbf{0} \\ \text{(III)} & \text{kinematical relation} & : & \mathbf{H} - \operatorname{Grad}\mathbf{u} & = & \mathbf{0} \end{array} \tag{2.1}$$

where the strain energy function $W = W\left(\mathbf{H}, (\mathbf{X}_i, i = 1, ..., n)\right)$ is a function of the strain tensor $\mathbf{H}$ and n internal variables $\mathbf{X}_i$ $(i = 1, ..., n)$ to model inelasticity. The vector $\mathbf{u}$ is the displacement vector. The tensor $\mathbf{P}$ represents the first Piola-Kirchhoff stress tensor and $\mathcal{A}_d$ a constant fourth order tensor to model the damping properties of the material. The quantity $\rho_0\,\mathbf{b}_v$ denotes a volume force (e. g. gravity), ρ_0 is the mass density in the undeformed configuration. The dot characterizes a derivative with respect to time. In a linear elasticity framework ($\boldsymbol{\sigma}$ stress tensor, $\mathcal{C}$ elasticity tensor, $\mathcal{D}$ tensor to model damping properties), above equations would take the form (I) $\operatorname{div}\boldsymbol{\sigma} + \rho_0\left(\mathbf{b}_v - \ddot{\mathbf{u}}\right) = \mathbf{0}$, (II) $\boldsymbol{\sigma} - \mathcal{C} : \boldsymbol{\varepsilon} - \mathcal{D} : \dot{\boldsymbol{\varepsilon}} = \mathbf{0}$, (III) $\boldsymbol{\varepsilon} - \operatorname{sym}\left(\operatorname{grad}\mathbf{u}\right) = \mathbf{0}$. The present element technology is based on the idea to fulfill these three equations only in weak form, i. e. not pointwise. In this way so-called incompatible modes, expressed by the so-called "enhanced" strain $\mathbf{H}_{\mathrm{enh}} = \mathbf{H} - \operatorname{Grad}\mathbf{u}$, can be introduced. They are constructed in such a way that the undesirable defect of low order finite elements ("locking") is avoided. In the following sections of the paper the compatible strain $\operatorname{Grad}\mathbf{u}$ is alternatively denoted as $\boldsymbol{H}_{\mathrm{comp}}$.

The equations 2.1 are multiplied with test functions $\delta\mathbf{u}$, $\delta\mathbf{H}$ and $\delta\mathbf{P}$, respectively, followed by an integration over the domain under investigation (B_0). Assuming further that $\mathbf{P}$ is constant within the element, we can finally eliminate the independent stress field and arrive at two equations of weak form:

$$g_1\left(\mathbf{u}, \mathbf{H}_{\mathrm{enh}}\right) = \int_{B_0} \left(\frac{\partial W}{\partial \mathbf{H}} + \mathcal{A}_d : \dot{\mathbf{H}}\right) : \operatorname{Grad}\delta\mathbf{u}\; dV + \int_{B_0} \rho_0\,\ddot{\mathbf{u}} \cdot \delta\mathbf{u}\; dV - g_{\mathrm{ext}} \tag{2.2}$$

$$g_2\left(\mathbf{u}, \mathbf{H}_{\mathrm{enh}}\right) = \int_{B_0} \left(\frac{\partial W}{\partial \mathbf{H}} + \mathcal{A}_d : \dot{\mathbf{H}}\right) : \delta\mathbf{H}_{\mathrm{enh}}\; dV = 0 \tag{2.3}$$

where g_{ext} is a short hand notation for the virtual work of the external loading. Obviously, the stress-like strain-dependent quantity

$$\bar{\mathbf{P}} = \frac{\partial W}{\partial \mathbf{H}} + \mathcal{A}_d : \dot{\mathbf{H}} \tag{2.4}$$

takes over the role of the originally introduced stress $\mathbf{P}$. Due to the fact that $\mathbf{P}$ has been eliminated, we can simplify notation by omitting the bar in what follows: $\mathbf{P} = \bar{\mathbf{P}}$.

3 Interpolation

The present paper is restricted to 2D problems (assumption of plane strain or axisymmetry). It is then suitable to work with the vector notation

$$\boldsymbol{H}^T = \{H_{11}, H_{22}, H_{12}, H_{21}, H_{33}\} \tag{3.1}$$

where H_{ij} $(i, j = 1, 2, 3)$ are the coefficients of $\boldsymbol{H} = \sum_{i=1}^{3}\sum_{j=1}^{3} H_{ij}\,\mathbf{e}_i \otimes \mathbf{e}_j$ with $\mathbf{e}_i$ $(i = 1, 2, 3)$ denoting a cartesian basis. In order to distinguish between the plane strain and the axisymmetric case, we further introduce with $\boldsymbol{H}_{\mathrm{PS}}$ the part of $\boldsymbol{H}^T = \{\boldsymbol{H}_{\mathrm{PS}}^T, H_{33}\}$ which is needed to model plane strain. The vector notation of the other second order tensors is constructed analogously, whereas the fourth order tensors are accordingly reduced to 5x5 matrices.

We now work with the interpolation (indicated by the index h)

$$\boldsymbol{H}_{\mathrm{PS}}^h = \underbrace{\left(\boldsymbol{B}_0 + \boldsymbol{j}_0\,\boldsymbol{L}_{\mathrm{hg}}\,\boldsymbol{M}_{\mathrm{hg}}\right)\boldsymbol{U}_e}_{= (\boldsymbol{H}_{\mathrm{PS}}^h)_{\mathrm{comp}} = \boldsymbol{B}\,\boldsymbol{U}_e} + \underbrace{\boldsymbol{j}_0\,\boldsymbol{L}_{\mathrm{enh}}\,\boldsymbol{W}_e}_{= (\boldsymbol{H}_{\mathrm{PS}}^h)_{\mathrm{enh}}}. \tag{3.2}$$

Here $\boldsymbol{B}_0$ denotes the constant part of the classical "$\boldsymbol{B}$"-matrix. The latter is used to compute the "compatible" part of $\boldsymbol{H}^h_{\rm PS}$ ($\boldsymbol{U}_e$ element vector of nodal displacements). The matrix $\boldsymbol{j}$ is given by

$$\boldsymbol{j} = \begin{bmatrix} \dfrac{\partial \xi}{\partial X} & \dfrac{\partial \eta}{\partial X} & 0 & 0 \\ 0 & 0 & \dfrac{\partial \xi}{\partial Y} & \dfrac{\partial \eta}{\partial Y} \\ \dfrac{\partial \xi}{\partial Y} & \dfrac{\partial \eta}{\partial Y} & 0 & 0 \\ 0 & 0 & \dfrac{\partial \xi}{\partial X} & \dfrac{\partial \eta}{\partial X} \end{bmatrix}. \tag{3.3}$$

The quantities ξ and η are local coordinates defined on the reference domain $\Omega_e = [-1,1] \times [-1,1]$, the cartesian coordinates X and Y refer to the undeformed configuration. A quantity evaluated at the centre of the element ($\boldsymbol{\xi} = \{\xi, \eta\}^T = \boldsymbol{0}$) is indicated by the index 0. The vector $\boldsymbol{W}_e$ contains the additional (internal) element degrees-of-freedom. The matrices $\boldsymbol{L}_{\rm hg}$, $\boldsymbol{M}_{\rm hg}$, $\boldsymbol{L}_{\rm enh}$ read

$$\boldsymbol{L}_{\rm hg} = \begin{bmatrix} \eta & 0 \\ \xi & 0 \\ 0 & \eta \\ 0 & \xi \end{bmatrix}, \quad \boldsymbol{M}_{\rm hg} = \begin{bmatrix} \boldsymbol{\gamma}^T & \boldsymbol{0} \\ \boldsymbol{0} & \boldsymbol{\gamma}^T \end{bmatrix}, \quad \boldsymbol{L}_{\rm enh} = \begin{bmatrix} \xi & 0 & 0 & 0 \\ 0 & \eta & 0 & 0 \\ 0 & 0 & \xi & 0 \\ 0 & 0 & 0 & \eta \end{bmatrix}. \tag{3.4}$$

The vector $\boldsymbol{\gamma}$ represents the so-called stabilization vector originally introduced in [14].

In contrast to the plane strain case ($H_{33} = 0$), we need to find a suitable interpolation for H_{33} for the axisymmetric deformation case. It is well-known that H_{33} can be computed with $H_{33} = \frac{u_1}{R}$ where u_1 is the displacement in X-direction and R the X-coordinate of the point where we wish to calculate H_{33}. Using the standard isoparametric bilinear shape functions for the interpolation of u_1, H_{33} becomes a linear function of ξ and η. So it is not necessary to consider here the incompatible modes which would yield an additional quadratic contribution. We arrive with $N_I = (1 + \xi\,\xi_I)\,(1 + \eta\,\eta_I)/4$ at

$$H^h_{33} = \frac{u^h_1}{\bar{R}} = \sum_{I=1}^{4} N_I\, U_{e\,2\,I-1}/(4\,\bar{R}). \tag{3.5}$$

The latter equation can be rewritten as $H^h_{33} = (\boldsymbol{B}_{3\,0} + \boldsymbol{B}_{3\,\xi}\,\xi + \boldsymbol{B}_{3\,\eta}\,\eta + \boldsymbol{B}_{3\,\xi\eta}\,\xi\,\eta)\,\boldsymbol{U}_e$ with the matrices $\boldsymbol{B}_{3\,0}$, $\boldsymbol{B}_{3\,\xi}$, $\boldsymbol{B}_{3\,\eta}$ and $\boldsymbol{B}_{3\,\xi\eta}$ being defined as

$$\begin{array}{lllllll} \boldsymbol{B}_{3\,0} & = & \{1,0,1,0,1,0,1,0\}/(4\,\bar{R}), & & \boldsymbol{B}_{3\,\xi} & = & \{-1,0,1,0,1,0,-1,0\}/(4\,\bar{R}) \\ \boldsymbol{B}_{3\,\eta} & = & \{-1,0,-1,0,1,0,1,0\}/(4\,\bar{R}), & & \boldsymbol{B}_{3\,\xi\eta} & = & \{1,0,-1,0,1,0,-1,0\}/(4\,\bar{R}) \end{array} \tag{3.6}$$

Although R certainly varies in the element, it is set equal to the constant

$$\bar{R} = \frac{1}{4}\,(X_1 + X_2 + X_3 + X_4), \tag{3.7}$$

where X_I ($I = 1, ..., 4$) are the X-coordinates of the four nodes.

4 Constitutive equations

One central idea of the present formulation is to replace the stress vector $\boldsymbol{P}$ by its Taylor expansion around a point on the line $\boldsymbol{\xi}_\star = \{0, \eta\}^T$ (see Figure 1).

$$\begin{aligned} \boldsymbol{P} &\approx \boldsymbol{P}_\star + \left.\frac{\partial \boldsymbol{P}}{\partial \xi}\right|_{\boldsymbol{\xi}=\boldsymbol{\xi}^\star} (\xi - 0) \\ &= \boldsymbol{P}_\star + \left.\frac{\partial \boldsymbol{P}}{\partial \boldsymbol{H}^h_{\mathrm{PS}}}\right|_{\boldsymbol{\xi}=\boldsymbol{\xi}^\star} ((\boldsymbol{j}_0\, \boldsymbol{L}'_{\mathrm{hg}}\, \boldsymbol{M}_{\mathrm{hg}})\, \boldsymbol{U}_e + \boldsymbol{j}_0\, \boldsymbol{L}'_{\mathrm{enh}}\, \boldsymbol{W}_e) \\ &\quad + \left.\frac{\partial \boldsymbol{P}}{\partial H^h_{33}}\right|_{\boldsymbol{\xi}=\boldsymbol{\xi}^\star} (\boldsymbol{B}_{3\,\xi}\, \xi + \boldsymbol{B}_{3\,\xi\eta}\, \xi\, \eta)\, \boldsymbol{U}_e \end{aligned} \tag{4.1}$$

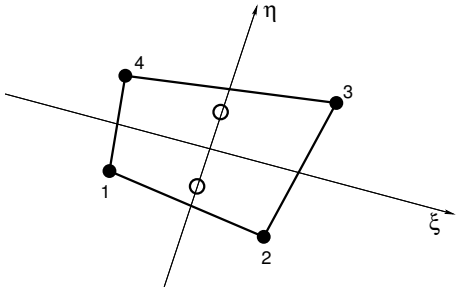

Figure 1: *Four-node element with coordinate system*

The expressions $\boldsymbol{L}'_{\mathrm{hg}}$ and $\boldsymbol{L}'_{\mathrm{enh}}$ are short notations for the partial derivatives $\partial \boldsymbol{L}_{\mathrm{hg}}/\partial\xi|_{\boldsymbol{\xi}=\boldsymbol{\xi}^\star}\ \xi$ and $\partial \boldsymbol{L}_{\mathrm{enh}}/\partial\xi|_{\boldsymbol{\xi}=\boldsymbol{\xi}^\star}\ \xi$, respectively. The relation 4.1 shows that $\boldsymbol{P}$ is now represented by a function which is linear in ξ. However, all three summands of $\boldsymbol{P}$ certainly still depend strongly non-linearly on the deformation. At this point one should be aware of the fact that a consistent linearization of these modified constitutive equations becomes highly complex. The computation of a so-called consistent tangent operator is necessary if the resulting finite element equation system is treated with an implicit solution scheme in combination with Newton's method. In the latter case, it is suitable to further simplify Equation 4.1 by replacing the partial derivatives of $\boldsymbol{P}$ with respect to $\boldsymbol{H}^h_{\mathrm{PS}}$ and H^h_{33} by constant matrices. Using additionally the assumption that $\boldsymbol{P}_{\mathrm{PS}}$ only depends on $\boldsymbol{H}^h_{\mathrm{PS}}$ whereas P_{33} is considered to depend on only H^h_{33} we finally obtain the constitutive equation

$$\boldsymbol{P} = \left\{ \begin{array}{c} \boldsymbol{P}^\star_{\mathrm{PS}} \\ P^\star_{33} \end{array} \right\} + \left[\begin{array}{cc} \boldsymbol{A}^\star_{\mathrm{PS}} & \boldsymbol{0} \\ \boldsymbol{0}^T & A^\star_{33} \end{array} \right] \left\{ \begin{array}{c} \boldsymbol{j}_0\, \boldsymbol{L}'_{\mathrm{hg}}\, \boldsymbol{M}_{\mathrm{hg}}\, \boldsymbol{U}_e + \boldsymbol{j}_0\, \boldsymbol{L}'_{\mathrm{enh}}\, \boldsymbol{W}_e \\ (\boldsymbol{B}_{3\,\xi}\, \xi + \boldsymbol{B}_{3\,\xi\eta}\, \xi\, \eta)\, \boldsymbol{U}_e \end{array} \right\} \tag{4.2}$$

The structure of the matrix $\boldsymbol{A}^\star_{\mathrm{PS}}$ is similar to the one of the elasticity matrix (with the Lamé constant Λ set equal to zero):

$$\boldsymbol{A}^\star_{\mathrm{PS}} = \left[\begin{array}{cccc} 2\,\mu^\star & 0 & 0 & 0 \\ 0 & 2\,\mu^\star & 0 & 0 \\ 0 & 0 & b\,\mu^\star & b\,\mu^\star \\ 0 & 0 & b\,\mu^\star & b\,\mu^\star \end{array} \right], \quad A^\star_{33} = 2\,\mu^\star \tag{4.3}$$

The factor b is equal to the ratio of the shorter with respect to the longer side length in one element. The parameter $\mu^\star$ equals the shear modulus if elastic material behaviour is considered. In plasticity we define the modulus $\mu^\star = \mu\, \widetilde{H}/(\widetilde{H} + E)$ where $\widetilde{H}$ represents the hardening

modulus at the onset of plastification (accumulated strain zero). For more details about the derivation of $\mu^\star$ and b see the discussion in [11], [15] and [12].

To conclude it should be mentioned that the influence of the second summand in Equation 4.2 vanishes with increasing number of elements. The material behaviour is dominated by the part $\boldsymbol{P}^\star$ which is left unchanged if one compares with the standard formulation. The second term yields the so-called "hourglass cernel" the choice of which is relatively arbitrary. Note that we provide here a physically-based form such that the "hourglass parameter" $\mu^\star$ does not have to be chosen manually.

5 Derivation of element matrices and vectors

The modified constitutive equations 4.2 are now inserted into the weak forms 2.3. Additionally, it is important to mention that the determinant J of the Jacobi matrix $\boldsymbol{J} = \partial \boldsymbol{X}/\partial \boldsymbol{\xi}$ (with $\boldsymbol{X} = \{X, Y\}^T$) is always evaluated in the centre of the element. The error introduced by this approximation vanishes with increasing number of elements. On the other hand we gain the important advantage that many terms drop out of the formulation.

5.1 Computation of internal element variables

From the second part of the weak form which has to be fulfilled elementwise one obtains

$$\boldsymbol{R}_w\,(\boldsymbol{U}_e, \boldsymbol{W}_{e\,\eta}) = \int_{\eta=-1}^{\eta=1} (\boldsymbol{L}_{\mathrm{enh}}^{\bullet\star})^T\, \boldsymbol{j}_0^T\, \boldsymbol{P}_{\mathrm{PS}}^\star\; J_0\, 2\, t\, d\eta = \boldsymbol{0} \tag{5.1}$$

where the matrix $\boldsymbol{L}_{\mathrm{enh}}^{\bullet\star}$ is computed with

$$(\boldsymbol{L}_{\mathrm{enh}}^{\bullet\star})^T = \begin{bmatrix} 0 & \eta & 0 & 0 \\ 0 & 0 & 0 & \eta \end{bmatrix}. \tag{5.2}$$

The letter t indicates the thickness of the element if we deal with the plane strain case. For axisymmetry t reads $t = 2\,\pi\,\bar{R}$. The vector of the internal element variables $\boldsymbol{W}_e^T = \{W_{e\,1}, W_{e\,2}, W_{e\,3}, W_{e\,4}\}^T$ can be split into two parts. Two of the four internal element variables ($W_{e\,1}$ and $W_{e\,3}$, included in $\boldsymbol{W}_{e\,\xi} = \{W_{e\,1},\, W_{e\,3}\}^T$) are never explicitly determined because the vector $\boldsymbol{W}_{e\,\xi}$ can be expressed in terms of the nodal degrees-of-freedom:

$$\boldsymbol{W}_{e\,\xi} = -\boldsymbol{K}_{ww}^{-1}\, \boldsymbol{K}_{wu}\, \boldsymbol{U}_e \tag{5.3}$$

The matrices $\boldsymbol{K}_{ww}$ and $\boldsymbol{K}_{wu}$ read

$$\begin{aligned} \boldsymbol{K}_{ww} &= \int_{\xi=-1}^{\xi=1} (\boldsymbol{L}_{\mathrm{enh}}^{\prime\star})^T\, \boldsymbol{j}_0^T\, \boldsymbol{A}_{\mathrm{PS}}^\star\, \boldsymbol{j}_0\, \boldsymbol{L}_{\mathrm{enh}}^{\prime\star}\; J_0\, 2\, t\, d\xi \\ \boldsymbol{K}_{wu} &= \int_{\xi=-1}^{\xi=1} (\boldsymbol{L}_{\mathrm{enh}}^{\prime\star})^T\, \boldsymbol{j}_0^T\, \boldsymbol{A}_{\mathrm{PS}}^\star\, \boldsymbol{j}_0\, \boldsymbol{L}_{\mathrm{hg}}^{\prime}\, \boldsymbol{M}_{\mathrm{hg}}\; J_0\, 2\, t\, d\xi := \boldsymbol{K}_{uw}^T \end{aligned} \tag{5.4}$$

with $(\boldsymbol{L}_{\mathrm{enh}}^{\prime\star})^T$ being defined as

$$(\boldsymbol{L}_{\mathrm{enh}}^{\prime\star})^T = \begin{bmatrix} \xi & 0 & 0 & 0 \\ 0 & 0 & \xi & 0 \end{bmatrix}. \tag{5.5}$$

In summary, the relation 5.1 represents a non-linear equation to determine the internal variables $\boldsymbol{W}_{e\,\eta} = \{W_{e\,2}, W_{e\,4}\}^T$ at the element level. The integration over η has to be performed numerically, i.e. the integrand has to be evaluated at (at least) two Gauss points located on the line $\boldsymbol{\xi}^\star = \{0, \eta\}^T$ (see the circled positions in Figure 1). Since $\boldsymbol{R}_w$ depends on $\boldsymbol{U}_e$ the solution of Equation 5.1 has to be embedded in the solution of the "global" finite element equations to be derived in what follows.

5.2 Derivation of the global equation system

The first part of the weak form yields after several calculation steps the relation

$$\begin{aligned} \tilde{g}_{1\,e} &= \delta\boldsymbol{U}_e^T\,(\boldsymbol{R}^0_{u\,\mathrm{PS}} + \boldsymbol{R}^0_{u\,33} + \boldsymbol{R}^{\mathrm{hg}}_{u\,\mathrm{PS}} + \boldsymbol{R}^{\mathrm{hg}}_{u\,33} + \boldsymbol{D}_e\,\dot{\boldsymbol{U}}_e + \boldsymbol{M}_e\,\ddot{\boldsymbol{U}}_e \\ &\quad + (\boldsymbol{K}^{\mathrm{hg}}_{uu\,\mathrm{PS}} + \boldsymbol{K}^{\mathrm{hg}}_{uu\,33})\,\boldsymbol{U}_e + \boldsymbol{K}_{uw}\,\boldsymbol{W}_{e\,\xi}) \end{aligned} \tag{5.6}$$

The first two summands are the parts of the classical residual force vector computed by means of the constant $\boldsymbol{B}$-matrices $\boldsymbol{B}_0$ and $\boldsymbol{B}_{3\,0}$, respectively:

$$\boldsymbol{R}^0_{u\,\mathrm{PS}} = \int_{\eta=-1}^{\eta=1} \boldsymbol{B}_0^T\,\boldsymbol{P}^\star_{\mathrm{PS}}\,J_0\,2\,t\,d\eta, \quad \boldsymbol{R}^0_{u\,33} = \int_{\eta=-1}^{\eta=1} \boldsymbol{B}_{3\,0}^T\,P^\star_{33}\,J_0\,2\,t\,d\eta \tag{5.7}$$

The parts $\boldsymbol{R}^{\mathrm{hg}}_{u\,\mathrm{PS}}$ and $\boldsymbol{R}^{\mathrm{hg}}_{u\,33}$ would also appear in a fully integrated element. They take here the forms

$$\boldsymbol{R}^{\mathrm{hg}}_{u\,\mathrm{PS}} = \int_{\eta=-1}^{\eta=1} \boldsymbol{M}^T_{\mathrm{hg}}\,(\boldsymbol{L}^{\bullet\star}_{\mathrm{hg}})^T\,\boldsymbol{j}_0^T\,\boldsymbol{P}^\star_{\mathrm{PS}}\,J_0\,2\,t\,d\eta, \quad \boldsymbol{R}^{\mathrm{hg}}_{u\,33} = \int_{\eta=-1}^{\eta=1} \eta\,\boldsymbol{B}_{3\,\eta}^T\,P^\star_{33}\,J_0\,2\,t\,d\eta \tag{5.8}$$

The computation of the element damping matrix $\boldsymbol{D}_e$ and the element mass matrix $\boldsymbol{M}_e$ is carried out as in classical displacement-based formulations, see the common text books [16] or [17]. If finally remains to determine the matrices $\boldsymbol{K}^{\mathrm{hg}}_{uu\,\mathrm{PS}}$ and $\boldsymbol{K}^{\mathrm{hg}}_{uu\,33}$:

$$\begin{aligned} \boldsymbol{K}^{\mathrm{hg}}_{uu\,\mathrm{PS}} &= \int_{\xi=-1}^{\xi=1} \boldsymbol{M}^T_{\mathrm{hg}}\,(\boldsymbol{L}'_{\mathrm{hg}})^T\,\boldsymbol{j}_0^T\,\boldsymbol{A}^\star_{\mathrm{PS}}\,\boldsymbol{j}_0\,\boldsymbol{L}'_{\mathrm{hg}}\,\boldsymbol{M}_{\mathrm{hg}}\,J_0\,2\,t\,d\xi \\ \boldsymbol{K}^{\mathrm{hg}}_{uu\,33} &= \frac{4}{3}\,\boldsymbol{B}^T_{3\,\xi} A^\star_{33}\,\boldsymbol{B}_{3\,\xi}\,J_0\,t + \frac{4}{3}\,\boldsymbol{B}^T_{3\,\eta} A^\star_{33}\,\boldsymbol{B}_{3\,\eta}\,J_0\,t + \frac{4}{9}\,\boldsymbol{B}^T_{3\,\xi\eta} A^\star_{33}\,\boldsymbol{B}_{3\,\xi\eta}\,J_0\,t \end{aligned} \tag{5.9}$$

Using Equation 5.3, the second line of Equation 5.6 reduces to $(\boldsymbol{K}^{\mathrm{hg}}_{uu\,\mathrm{PS}} + \boldsymbol{K}^{\mathrm{hg}}_{uu\,33} - \boldsymbol{K}_{uw}\,\boldsymbol{K}^{-1}_{ww}\,\boldsymbol{K}_{wu})\,\boldsymbol{U}_e := \boldsymbol{K}_{\mathrm{stab}}\,\boldsymbol{U}_e$. Due to the fact that the integrands included in the matrices $\boldsymbol{K}^{\mathrm{hg}}_{uu\,\mathrm{PS}}$, $\boldsymbol{K}^{\mathrm{hg}}_{uu\,33}$, $\boldsymbol{K}_{ww}$ and $\boldsymbol{K}_{uw}$ are polynomials in ξ, the corresponding integrations can be performed analytically. Therefore we do not need any numerical integration procedure to determine the "hourglass stabilization matrix" $\boldsymbol{K}_{\mathrm{stab}}$. One finally arrives at the relation

$$\tilde{g}_{1\,e} = \delta\boldsymbol{U}_e^T\,(\boldsymbol{R}_u\,(\boldsymbol{U}_e, \boldsymbol{W}_{e\,\eta}) + \boldsymbol{D}_e\,\dot{\boldsymbol{U}}_e + \boldsymbol{M}_e\,\ddot{\boldsymbol{U}}_e + \boldsymbol{K}_{\mathrm{stab}}\,\boldsymbol{U}_e), \tag{5.10}$$

where the abbreviation

$$\boldsymbol{R}_u := \boldsymbol{R}^0_{u\,\mathrm{PS}} + \boldsymbol{R}^0_{u\,33} + \boldsymbol{R}^{\mathrm{hg}}_{u\,\mathrm{PS}} + \boldsymbol{R}^{\mathrm{hg}}_{u\,33} \tag{5.11}$$

has been introduced.

The element quantities are assembled to yield the global time-continuous differential equation system

$$\boldsymbol{R}_{u\,G}\left(\boldsymbol{U}\right) + \boldsymbol{K}_{\mathrm{stab}\,G}\,\boldsymbol{U} + \boldsymbol{D}_G\,\dot{\boldsymbol{U}} + \boldsymbol{M}_G\,\ddot{\boldsymbol{U}} - \boldsymbol{F}_{\mathrm{ext}} = \boldsymbol{0} \tag{5.12}$$

where the index G refers to the global level and $\boldsymbol{U}$ denotes the *global* vector of nodal displacements. $\boldsymbol{F}_{\mathrm{ext}}$ is the global external load vector. It is assumed that the internal element variables $\boldsymbol{W}_{e\,\eta}$ are determined at the element level such that they do not enter the global equation system.

The time discretization can be carried out with any implicit or explicit integration scheme, such as e.g. the Newmark method, the generalized α-method (implicit schemes) or the method of finite differences (explicit scheme). Note that only the former procedure requires the solution of a non-linear equation system.

5.3 Summary

To conclude we summarize the differences of the present stabilized reduced integration technique with respect to standard displacement-based approaches as well as alternative locking-free element formulations.

Implementation:

- Instead of a full (2x2) integration the present formulation requires only two Gauss points (located on the line $\boldsymbol{\xi}^{\star} = \{0, \eta\}$).
- We have to solve the non-linear equation $\boldsymbol{R}_w = \boldsymbol{0}$ at the element level. These are two scalar equations. Obviously the computational effort caused by this additional step is very small.
- The hourglass stabilization matrix which is given by an analytical expression has to be computed once per time step in an extra subroutine.
- The use of the modified constitutive equations means to work with an “anisotropic” ansatz. For this reason in each element a coordinate transformation has to be carried out which clearly identifies the thickness direction.
- The formulation can be easily implemented into a commercial finite element code. In contrast to the standard displacement approach the storage of the internal element variables has to be performed. This is, however, also necessary for the enhanced strain method which is already commonly offered in commercial finite element tools. The additional element variables are not needed for thin shell geometries.

User:

- Neither the input nor the computation requires special care. For certain applications a manual choice of the hourglass parameter $\mu^{\star}$ and the shear reduction factor b would be useful.

Advantages:

- The element is free of volumetric, shear and membrane locking. This property is usually only achieved in the framework of highly sophisticated shell formulations.
- Due to the absence of shear locking, thin shell computations can be carried out with only one element over the thickness. First of all this reduces the computational effort enormously. Secondly, the ratio of the element side lengths is less extreme such that the critical time step for the explicit time integration is significantly increased.

  Thus both, the number of elements and the number of time steps can be reduced!
- The element possesses four nodes. The extension of the structure in thickness direction is correctly displayed. This property proves to be in particular advantageous for the contact modelling.
- It is trivial to take several elements over the thickness. Usually this is necessary for the modelling of thick structures.
- The elements can be easily coupled to classical 2D elements.

6 Examples

6.1 Cylindrical shell under line load

Geometry and boundary conditions for this example are plotted in Figure 2a. All quantities are given in N and mm. The material is elastic (with the parameters given in Section 5.4.1 [18]). We investigate first a cylindre with a rather small length/thickness ratio ($L/t = 10$). The discretization is chosen in such a way that the element side length ratio is equal to one. The load is applied in 100 equal steps (inertia effects neglected). For such a so-called thick shell it cannot be expected that one element over the thickness is sufficient. The results of the present element formulation (Q1SPs) are compared to the ones obtained with the reduced integration technique Q1SPe [15] where the special shell-like deformation behaviour is not taken into account. The study of convergence (Figure 2b) shows that the use of Q1SPs yields much better convergence behaviour. A discretization with 4x40 elements is already sufficient to obtain an accurate result. It becomes also evident that the choice of $\mu^\star$ influences the convergence behaviour but not the final result ("mopt"$= \mu$). It is recommended to choose $\mu^\star$ ("m") as small as possible. However, too small values make the element rather sensitive to severe mesh distortion. If the internal element variables are set equal to zero we obtain the result described by "oenh". Practically then we work with a thin shell element technology which is (as expected) not suitable for thick shell applications.

For a very thin shell geometry with $R/t = 1000$ the element shows an outstanding convergence behaviour. The load is applied in the following way: 10 x 0.001, 19 x 0.01, 20 x 0.04. We

obtain for the maximum displacement in horizontal direction the results: 10x1 el.: 2.96, 20x1 el.: 3.00, 40x1 el.: 3.02, 80x1 el.: 3.03 ($\mu^\star = 4\,\mu$). These results do not vary if the discretization in thickness direction is refined. Further the enhanced degrees-of-freedom are not needed here, i.e. they do not influence the results. It can be concluded that we obtain a very strong *thin* shell element if the additional element degrees-of-freedom are set equal to zero. Interestingly also the factor b has a very small influence on the result. In contrast, Q1SPe reacts very sensitively, it is clearly not suitable for such thin structures.

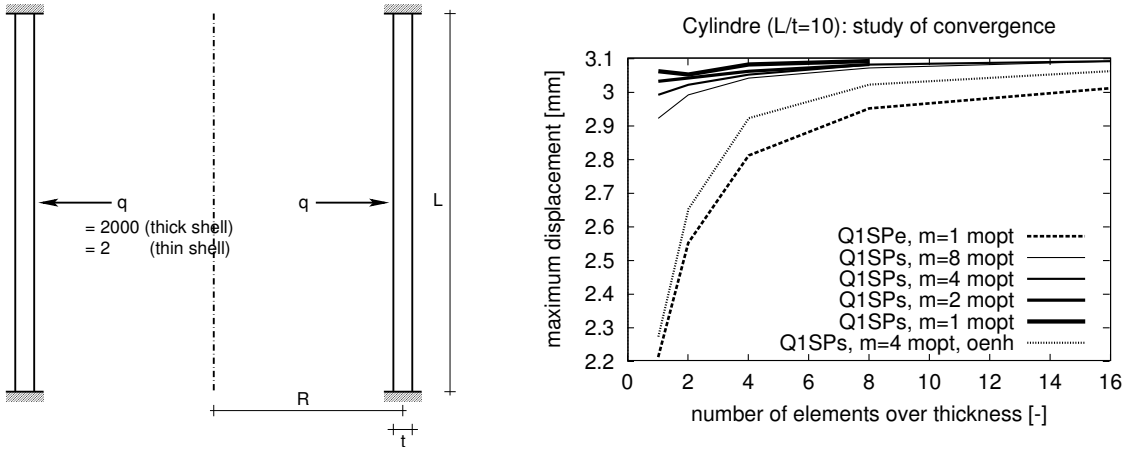

Figure 2: *(a) Geometry and boundary conditions of a cylindrical shell*
(b) Study of convergence (shell with $R/t = 10$)

6.2 Pinched cylinder with end diaphragms

Another challenging example to test the bending behaviour is the so-called “cola can”. We work here with a general shell geometry, i.e. the eight-noded Q1SPs. For symmetry reasons, only one eighth of the structure has to be discretized (see Figure 3a). The displacement w_A at node A ($X_1 = X_3 = 0\,\mathrm{mm}$, $X_2 = 301.5\,\mathrm{mm}$) is controlled in such a way that it moves downwards (w_A). Besides the symmetry conditions applied on the planes $X_1 = 0\,\mathrm{mm}$, $X_2 = 0\,\mathrm{mm}$ and $X_3 = 0\,\mathrm{mm}$ we have constraints in X_1- and X_2-direction (diaphragm) on the plane $X_3 = 300\,\mathrm{mm}$. The material is assumed to be elasto-plastic, see [11] for more details.

In Figure 4a, the contours of the yield criterion Φ are plotted on a deformed configuration of the structure ($w_A = 200\,\mathrm{mm}$). Figure 4b shows the plastic zone. A study of convergence is plotted in Figure 3b. The comparison with QM1/E12 (see Wriggers et al. [19]) and the 6-parameter shell formulation of Eberlein & Wriggers [20] shows that the convergence behaviour is very satisfactory. Concerning the choice of the load steps it should be mentioned that with increasing number of elements also the problem of wrinkling, i. e. structural instability, arises. So for the discretization 64x2x32 the load step had to be partially reduced to $\Delta w_A = 0.5\,\mathrm{mm}$. In comparison, for the mesh 32x2x16, the computation could be performed with $\Delta w_A = 2\,\mathrm{mm}$.

6.3 Electromagnetic forming

The following example serves to validate Q1SPs in the context of high speed forming. For this purpose we carry out the finite element simulation of an electromagnetic forming process.

The tool coil creates a magnetic field which introduces an electric current in the sheet metal. Due to the interaction with the magenetic field Lorentz forces are generated and the workpiece deforms. The experimental procedure yields the distribution of the Lorentz forces in normal and tangential direction at discrete points in space (radius r, thickness coordinate y) and time.

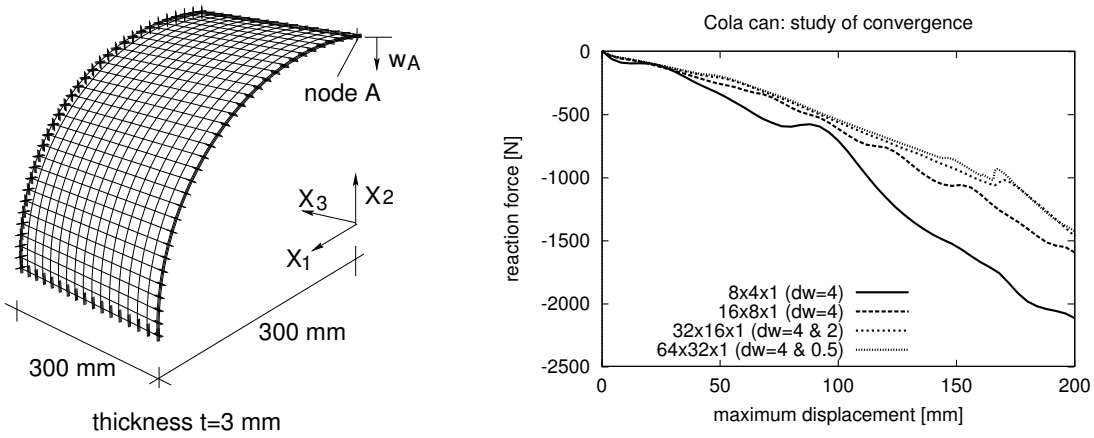

Figure 3: *Pinched cylinder (a) Geometry, discretization, boundary conditions (b) Study of convergence*

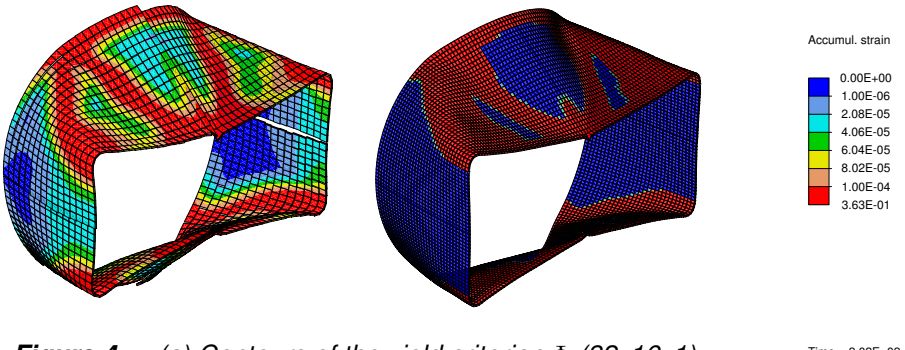

Figure 4: *(a) Contours of the yield criterion Φ (32x16x1) (b) Plastic zone (64x32x1)*

To prepare the data for the input into the finite element program system, each point $P = (r, y)$ has to be associated with the closest Gauss point in the structure discretized with finite elements. This is suitably done by means of a search procedure to find the element which includes the point P followed by a computation of the distances to the Gauss points of the corresponding element. In the FE computation, the element routine reads at each time the Lorentz force components for this Gauss point. The present time is compared to the discrete times where the function is prescribed. In between a linear dependence on time is assumed. The Lorentz force acts together with the mass inertia as volume force on the finite element system.

Interestingly, in comparison to the previous examples, the shear locking plays here only a subordinate role. This might be attributed to the fact that the structural behaviour is membrane-like, i.e. bending plays only a subordinate role. Nevertheless we have still the important advantage that the computation can be performed with only one element over the thickness, something not possible with Q1SPe [13]. In Figure 5, the computed deformed configurations

with the present code (FEAP, Finite Element Analysis Program) are compared to the results achieved with MARC [13], however using a slightly different hardening rule in the elastoplastic material law. Obviously a highly satisfactory agreement is obtained.

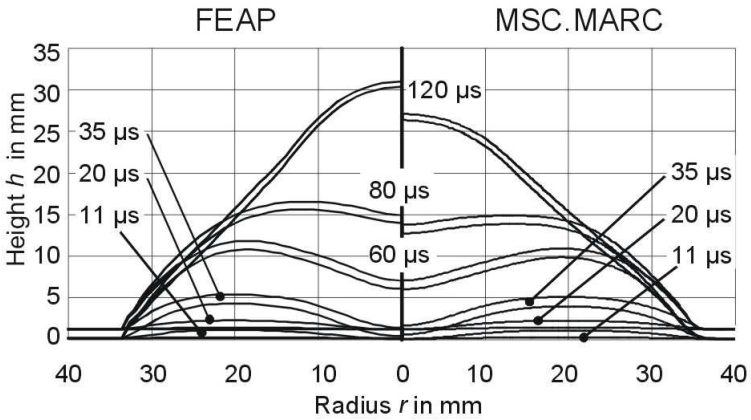

Figure 5: *Intermediate stages of the simulation*

6.4 Deep drawing

We finally investigate the deep drawing of a sheet metal of the radius a and the thickness $3.7714 \cdot 10^{-3}\, a$. More details about the geometry and the boundary conditions cannot be documented due to secrecy agreements. The structure is discretized with 60 elements in radial direction and only one element over the thickness. The frictional contact between the punch and the workpiece is taken into account by means of a penalty formulation. The intermediate stages of the deep drawing process are shown in Figure 6. The contours refer to the accumulated plastic strain.

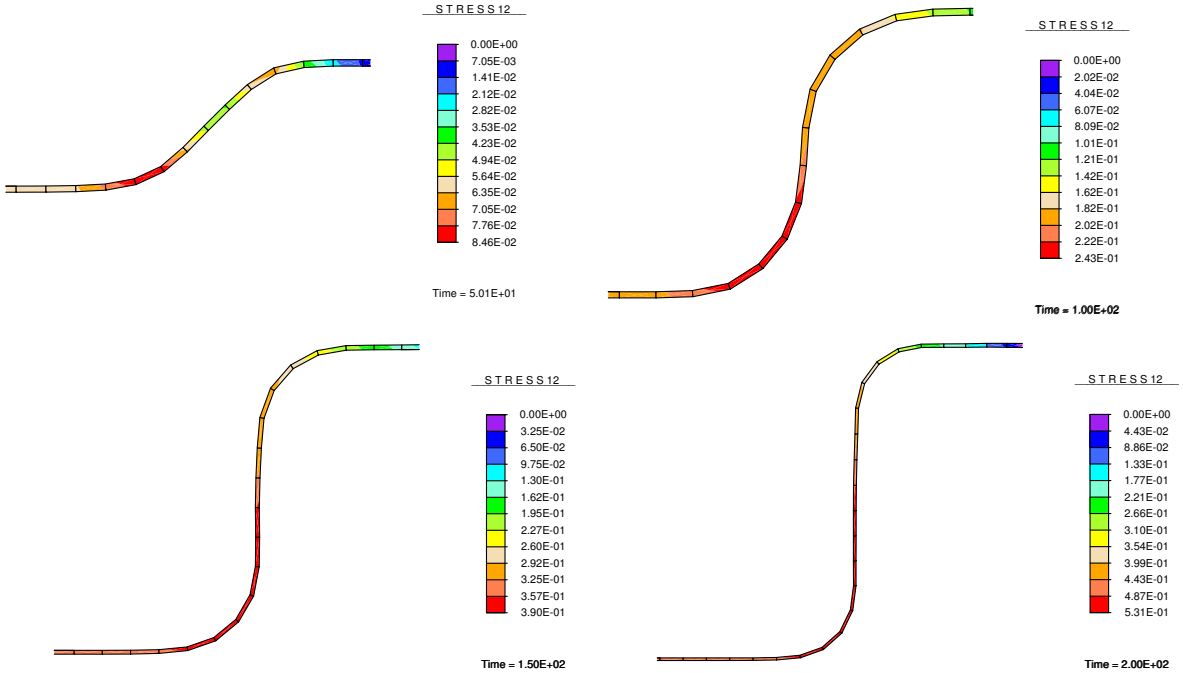

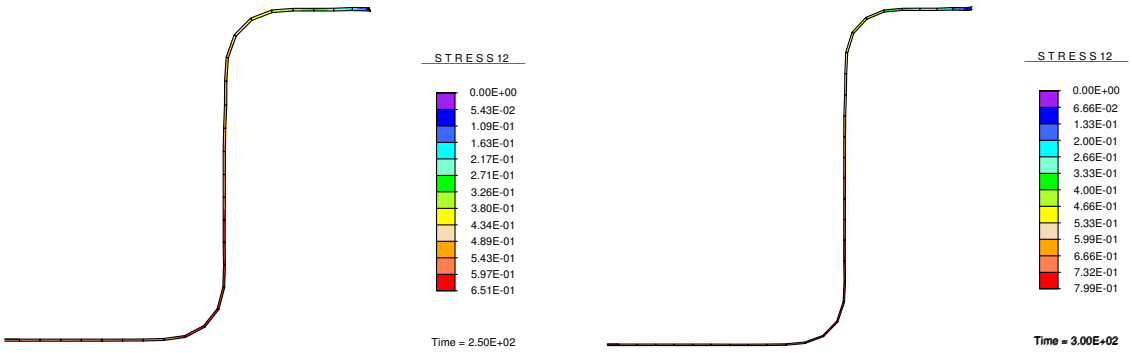

Figure 6: *Intermediate stages in deep drawing simulation*

The simulation can be performed with 3000 implicit steps and takes about 10 min on a modern personal computer. Interestingly the thick shell formulation behaves in this application rather sensitively. The computation can be performed robustly only with the thin shell formulation (without the internal element degrees-of-freedom). However, the radius/thickness ratio of the sheet metal is such that the thin shell assumption is easily justified, especially if one takes the extreme thinning of the structure in the last stages into account.

Future work should be directed to more complex forming applications and a comparison with experimental data.

References

[1] *Simo, J.C., F. Armero*, Geometrically nonlinear enhanced strain mixed methods and the method of incompatible modes. *International Journal for Numerical Methods in Engineering* **33**, 1413–1449, 1992.

[2] *Simo, J.C., F. Armero, R.L. Taylor*, Improved versions of assumed enhanced strain tri-linear elements for 3D finite deformation problems. *Computer Methods in Applied Mechanics and Engineering* **110**, 359–386, 1993.

[3] *Cao, Y.P., N. Hu, J. Lu, H. Fukunaga, Z.H. Yao*, A 3D brick element based on Hu-Washizu variational principle for mesh distortion. *International Journal for Numerical Methods in Engineering* **53**, 2529–2548, 2002.

[4] *Areias, P.M.A., J.M.A. César de Sá, C.A. Conceicao António, A.A. Fernandes*, Analysis of 3D problems using a new enhanced strain hexahedral element. *International Journal for Numerical Methods in Engineering* **58**, 1637–1682, 2003.

[5] *Belytschko, T., L.P. Bindeman*, Assumed strain stabilization of the eight node hexahedral element, *Computer Methods in Applied Mechanics and Engineering* **105**, 225–260, 1993.

[6] *Liu, W.K., Y. Guo, S. Tang, T. Belytschko*, A multiple-quadrature eight-node hexahedral finite element for large deformation elastoplastic analysis, *Computer Methods in Applied Mechanics and Engineering* **154**, 69–132, 1998.

[7] *Puso, M.A.*, A highly efficient enhanced assumed strain physically stabilized hexahedral element, *International Journal for Numerical Methods in Engineering* **49**, 1029–1064, 2000.

[8] *Reese, S., B.D. Reddy, P. Wriggers*, A new locking-free brick element technique for large deformation problems in elasticity, *Computer and Structures* **75**, 291–304, 2000.

[9] *Cardoso, R.P.R., J.-W. Yoon, J.J. Grácio, F. Barlat, J.M.A. César de Sá*, Development of a one point quadrature shell element for nonlinear applications with contact and anisotropy, *Computer Methods in Applied Mechanics and Engineering* **191**, 5177–5206, 2002.

[10] *Legay, A., A. Combescure*, Elastoplastic stability analysis of shells using the physically stabilized finite element SHB8PS, *International Journal for Numerical Methods in Engineering* **57**, 1299–1322, 2003.

[11] *Reese, S.*, On a physically stabilized one point finite element formulation for three-dimensional finite elasto-plasticity, submitted to *Computer Methods in Applied Mechanics and Engineering*, 2004.

[12] *Reese, S.*, On a new large deformation solid-shell concept based on reduced integration, submitted to *International Journal for Numerical Methods in Engineering*, 2004.

[13] *Kleiner, M., A. Brosius, H. Blum, F.-T. Suttmeier, M. Stiemer, B. Svendsen, J. Unger, S. Reese*, Benchmark simulation for coupled electromagnetic-mechanical metal forming processes, to be published in WGP.Annalen, 2004.

[14] *Belytschko, T., J.S.-J. Ong, W.K. Liu, J.M. Kennedy*, Hourglass control in linear and nonlinear problems, *Computer Methods in Applied Mechanics and Engineering* **43**, 251–276, 1984.

[15] *Reese, S.*, On a consistent hourglass stabilization technique to treat large inelastic deformations and thermo-mechanical coupling in plane strain problems, *International Journal for Numerical Methods in Engineering* **57**, 1095–1127, 2003.

[16] *Bathe, K.-J.*, *Finite-Elemente-Methoden*,Springer, Berlin, 1986.

[17] *Hughes, T.J.R.*, *The Finite Element Method*, Prentice-Hall, Englewood Cliffs, 1987.

[18] *Eberlein, R.*, Finite-Elemente-Konzepte für Schalen mit großen elastischen und plastischen Verzerrungen, Dissertation, Fachbereich Mechanik, Technische Universität Darmstadt, 1997.

[19] *Wriggers, P., R. Eberlein, S. Reese*, A comparison of three-dimensional and shell elements for finite plasticity, International Journal of Solids and Structures **33**, 3309–3326, 1996.

[20] *Eberlein, R., P. Wriggers*, Finite element concepts for finite elastoplastic strains and isotropic stress response in shells: theoretical and computational analysis, *Computer Methods in Applied Mechanics and Engineering* **171**, 243–279, 1999.